

GeneCS: Synthesizing Resource-Efficient Code Surgery for Arbitrary Quantum Stabilizer Codes

Junyu Zhou
University of Pennsylvania
Philadelphia, USA
junyuzh@seas.upenn.edu

Ali Javadi-Abhari
IBM Quantum
New York, USA
Ali.Javadi@ibm.com

Gushu Li
University of Pennsylvania
Philadelphia, USA
gushuli@seas.upenn.edu

Abstract

Efficiently realizing logical operations on general stabilizer codes remains a long-standing challenge in fault tolerant quantum computing. While code surgery provides a general framework with provable guarantees by joint logical measurements, existing constructions are largely theoretical and incur substantial ancilla overhead in practice. In this work, we propose GeneCS, a resource-efficient compiler for synthesizing code surgery protocols for arbitrary stabilizer codes. Our approach leverages structure-aware optimizations to eliminate redundancy in graph construction, dynamically balance expansion and congestion, and incorporate code degree constraints. Experimental results show that GeneCS achieves an average reduction of over 85% in ancillary qubits and checks for both single-code and cross-code logical operations, while preserving logical error rates. Moreover, our compiler scales to codes with more than 10^4 qubits with an amortized compilation time of about one second per instance. These results enable practical logical operations and efficient cross-code communication, thereby supporting the deployment of modern QLDPC codes and heterogeneous quantum architectures.

1 Introduction

Quantum error correction (QEC) [19] is a fundamental requirement for scalable fault-tolerant [20] quantum computing. Most practical QEC schemes are based on the stabilizer formalism, which provides a unified framework for describing a wide range of codes. Over the past decade, a diverse landscape of stabilizer codes has emerged, including topological codes [3] such as the surface code [16] and color codes [26], as well as more recent constructions such as Quantum Low-Density Parity-Check (QLDPC) codes [5], e.g., Bivariate Bicycle (BB) codes [4, 36]. These code families offer complementary advantages: surface codes enable efficient fault-tolerant logical operations with local interactions, while QLDPC codes provide significantly improved encoding rates and are attractive for quantum memory.

A key implication of this diversity is that practical fault-tolerant quantum computing is unlikely to rely on a single code family. Due to fundamental constraints on fault-tolerant universality [6, 13], efficient implementations of universal fault-tolerant quantum computing typically require combining multiple codes or switching between encoding schemes.

Emerging system-level studies further support this view, showing that leveraging different codes or platforms can significantly improve resource efficiency [14, 28, 32]. These trends highlight a fundamental requirement: *efficient cross-code communication*. Logical quantum information must be transferred across different encodings, and joint logical operations must be performed between them. Consequently, enabling *communication and logical operations across arbitrary stabilizer codes* becomes a central challenge for scalable fault-tolerant quantum computing.

This paper focuses on this challenge. In particular, we study how to realize fault-tolerant logical operations that enable cross-code communication, and more specifically, how to efficiently synthesize *code surgery* protocols for arbitrary stabilizer codes. Code surgery [8, 9, 12], a generalization of lattice surgery [24], provides a natural mechanism for implementing joint logical measurements and transferring logical information across arbitrary stabilizer codes. While lattice surgery on the surface code is well understood and highly optimized [15, 24, 27, 39], efficiently extending these techniques to general stabilizer codes remains an open challenge. Existing approaches are either general but inefficient—relying on conservative constructions that incur substantial ancilla overhead, with the first theoretical guarantees of QLDPC structure and distance preservation given in [35]—or specialized ad-hoc designs [35] that are limited to specific instances, as well as constructions that rely on expensive computations such as code distance checking [9, 25, 38], and thus do not scale.

This gap highlights a missing abstraction: *resource-efficient code surgery should be treated as a synthesis and optimization problem*. In particular, we observe that constructing code surgery protocols can be naturally formulated as a *graph synthesis problem*, where the ancilla system corresponds to a graph whose structure determines both correctness (e.g., distance preservation) and resource cost. Existing constructions [22, 35] follow rigid pipelines (expansion, decongestion, thickening, and cellulation) designed for analysis, but introduce significant redundancy when applied in practice. This motivates the need for a compiler that directly optimizes this graph structure.

To this end, we propose GeneCS, a compiler framework for synthesizing resource-efficient code surgery protocols for arbitrary stabilizer codes. As shown in Figure 1, GeneCS

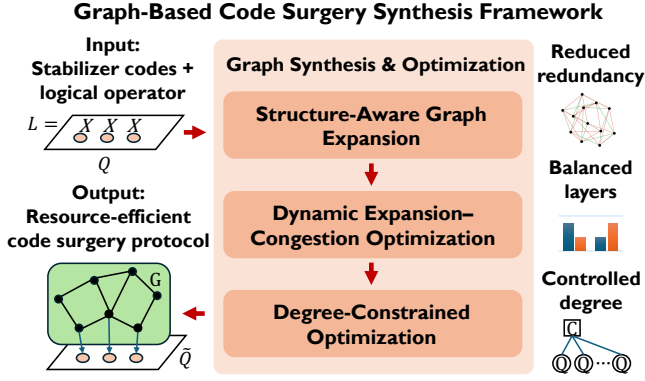


Figure 1. Overview of GeneCS workflow

treats code surgery construction as a graph optimization problem and systematically reduces redundancy across the entire pipeline. Our design is based on three key ideas. **First**, we propose a new graph expansion algorithm to leverage the connectivity already present in the initial path-matching structure, avoiding redundant edge additions introduced by independent expander constructions. **Second**, we introduce a dynamic cycle-tracking framework that monitors congestion during graph construction and identifies the optimal expansion-congestion trade-off point online, eliminating unnecessary thickening. **Third**, we incorporate degree constraints into the construction by enforcing qubit and check degree limits through load-aware cycle partitioning and generalized cellulation, yielding more efficient implementations.

Our experimental results show that GeneCS significantly reduces the resource overhead of code surgery constructions. For single-code logical measurements, our method achieves an average reduction of 86.7% in ancillary qubits and 85.8% in checks compared to the best baseline. For cross-code logical measurements, we observe consistent reductions of around 85%. These improvements are achieved without degrading logical error rates, while maintaining practical efficiency. Even for large codes with over 10^4 qubits, the amortized compilation time is approximately one second per instance.

Our major contributions can be summarized as follows:

1. **General and efficient code surgery synthesis.** We propose GeneCS, the first resource-efficient compiler for synthesizing code surgery protocols that realize logical operations across arbitrary stabilizer codes.
2. **Graph-based optimization framework.** We formulate code surgery synthesis as a graph optimization problem and introduce techniques that eliminate redundancy, balance expansion and congestion, and incorporate qubit degree constraints.
3. **Strong performance and scalability.** GeneCS achieves over 85% reduction in ancillary resources while

(a). Surface code (b). Code as graph

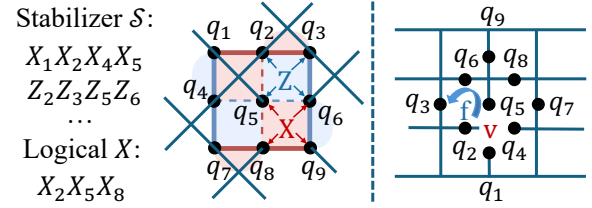


Figure 2. Example: surface code and its graph representation

preserving code distance and logical error rates, enabling efficient cross-code communication and scalable fault-tolerant quantum computing.

2 Preliminary

We provide a brief overview of the stabilizer formalism for quantum error-correcting codes and code surgery technique. For a general introduction to quantum computing, we refer the reader to [29].

2.1 Stabilizer Formalism

Let \mathcal{P}_n denote the n -qubit Pauli group. A stabilizer code [19] is defined by an abelian subgroup:

$$\mathcal{S} = \langle S_1, \dots, S_m \rangle \subset \mathcal{P}_n, \quad -I \notin \mathcal{S}.$$

The code space is the simultaneous $+1$ eigenspace of all stabilizers, given by:

$$\mathcal{C} = \{ |\psi\rangle : S|\psi\rangle = |\psi\rangle, \forall S \in \mathcal{S} \}.$$

States in \mathcal{C} are referred to as stabilizer states.

Logical operators are Pauli operators that preserve the code space but are not contained in the stabilizer group. Specifically, a Pauli operator $L \in \mathcal{P}_n$ is a logical operator if it commutes with all stabilizers:

$$LS = SL, \quad \forall S \in \mathcal{S},$$

and $L \notin \mathcal{S}$. Let $\mathcal{N}(\mathcal{S})$ denote the normalizer of $\mathcal{S} \in \mathcal{P}_n$. Then the logical Pauli operators correspond to equivalence classes in the quotient space $\mathcal{N}(\mathcal{S})/\mathcal{S}$. An example of the stabilizer and logical operator of a surface code is shown in Fig. 2(a).

2.2 Codes as Graphs: A Unifying Perspective

A key observation underlying this work is that the ancilla system constructed in code surgery admits a natural graph representation. This view provides an intuitive way to understand how stabilizers act on qubits and will be used throughout the paper. In particular, we adopt the following abstraction for the graph representation of an ancilla system:

- vertices correspond to $X(Z)$ -type stabilizer checks,
- edges correspond to physical qubits,
- cycles in the graph correspond to $Z(X)$ -type stabilizer checks.

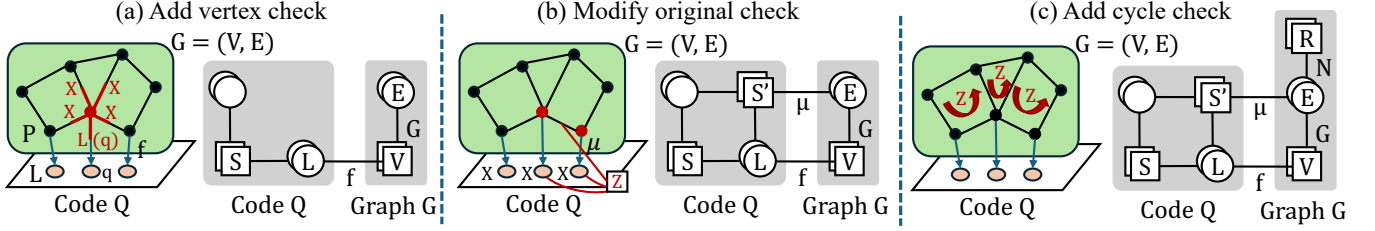


Figure 3. Ancilla system represented as a graph.

This representation allows us to translate QEC code structure into a combinatorial object, making it amenable to algorithmic optimization. This correspondence is due to the underlying CSS structure of the surgery system, where the graph for surgery can be interpreted as a low-dimensional chain complex, with vertices, edges, and cycles corresponding to 0-, 1-, and 2-cells, respectively. Under this correspondence, the action of stabilizers is encoded directly in the graph structure: each $X(Z)$ -type vertex check acts on all incident edges of a vertex, while each $Z(X)$ -type cycle check acts on the set of edges forming a cycle. As a result, the commutation structure of the code is reflected in the structure of the chain complex, where the composition of consecutive boundary operators vanishes.

To simply illustrate this abstraction, we use the surface code shown in Figure 2. On the left is a surface code patch, where red regions denote X -type stabilizers and blue regions denote Z -type stabilizers, each acting on a set of neighboring qubits (shown as black dots). This structure naturally admits a graph interpretation on the right. In this graph, vertices correspond to X -type stabilizers, edges correspond to physical qubits, and faces (i.e., cycles in the underlying graph) correspond to Z -type stabilizers. Under this mapping, each X stabilizer acts on the edges incident to a vertex, while each Z stabilizer acts on the edges along the boundary of a face. We can view the graph on the right as being overlaid onto the surface code patch on the left, establishing a one-to-one correspondence between graph elements and code structure.

This perspective makes explicit how the stabilizer structure is encoded combinatorially and serves as the basis for the graph-based formulation of code surgery. Importantly, it enables us to treat code surgery as a graph synthesis problem, where optimizing the graph directly improves resource efficiency.

2.3 General Code Surgery

Code surgery [8, 12, 22, 35] realizes logical operations by measuring logical operators through an ancilla system. Intuitively, it transforms a high-weight logical operator into a set of low-weight stabilizer measurements that can be executed fault-tolerantly. At a high level, the procedure works as follows. Starting from an original code Q , we introduce an ancilla system that interacts with the support of a logical

operator L (i.e., the qubits involved in L). By appropriately coupling the ancilla system to the code, we obtain a deformed code \tilde{Q} in which L is promoted to a stabilizer and can be measured through the syndrome measurement of \tilde{Q} .

From the graph perspective introduced in the previous section, this procedure corresponds to attaching an ancilla graph to the logical operator. The vertices of the graph introduce new checks that couple to L , while the cycles of the graph introduce additional constraints that fix the gauge degrees of freedom. Meanwhile, some of the original checks are modified to ensure that all stabilizers remain commuting. As a result, the logical operator is no longer supported solely on the original qubits, but is distributed across the ancilla graph and can be measured via local checks.

We now formally define the graph for code surgery as shown in Figure 3. We denote the original stabilizer code by Q with stabilizer group \mathcal{S} . Let L be the logical operator of interest, represented as a Pauli string supported on a set of physical qubits q_i . We write $L(q_i)$ to denote the Pauli operator acting on the qubit q_i . Then the ancilla system is represented as a graph $G = (V, E)$ attached to the original code Q , defined via a bijective map $f : L \rightarrow P$, which connects a subset of vertices, referred to as ports P , to the support of the logical operator. This construction is illustrated in Fig. 3(a).

We now formally define the code surgery construction by interpreting the graph $G = (V, E)$ together with the original code Q as a deformed stabilizer code \tilde{Q} .

First, we introduce vertex checks. We assume that we are measuring an X logical operator; the case of measuring a Z operator follows by simply exchanging the roles of X and Z in the following discussion. For non-CSS stabilizer codes, no modification is required. Each vertex $v \in V$ corresponds to a check, and each edge $e \in E$ corresponds to a qubit. For $v \in V$, if $v \notin P$, we add the stabilizer $A_v = \prod_{e \ni v} X(e)$ to the deformed stabilizer group $\tilde{\mathcal{S}}$; if $v = f(q) \in P$, we instead add $A_v = L(q) \prod_{e \ni v} X(e)$ to $\tilde{\mathcal{S}}$. An example is illustrated in Fig. 3(a), where the vertex highlighted in red enforces an X -parity check on its adjacent edges ($e \ni v$), together with the Pauli operator on the logical support of L specified by the map f . Since we consider connected graphs, the product of all vertex checks yields the logical operator to be measured. An alternative high-level representation is shown on the right of Fig. 3(a), where double squares denote checks and

double circles denote qubits. After introducing the vertex checks, check V is connected to the logical operator L via the map f , and to the qubit E according to the graph G .

Second, we modify the original stabilizers to ensure that the deformed stabilizer group remains commuting. This is necessary because the vertex checks introduced in the previous step may anti-commute with some stabilizers in the original code. The procedure is known as constructing **path-matching graph**. For each stabilizer $S \in \mathcal{S}$, let $K(S, L)$ denote the set of qubits q on which $S(q)$ and $L(q)$ anti-commute. Note that $|K(S, L)|$ must be even. If $K(S, L) = \emptyset$, we directly include S in $\tilde{\mathcal{S}}$. Otherwise, let $\mu(S, L)$ be a path matching of $f(K(S, L))$ in G , and define the modified stabilizer $\tilde{S} = S \prod_{e \in \mu(S, L)} Z(e)$, which is then added to $\tilde{\mathcal{S}}$. An example is shown in Fig. 3(b), where the logical operator is $L = XXX$, and a stabilizer $S = ZZ$ anti-commutes with two X operators in L 's physical support on the right. These two physical qubits form the set $K(S, L)$, and $f(K(S, L))$ corresponds to the two highlighted red vertices in G . A valid path matching $\mu(S, L)$ can be chosen as the edge connecting these two vertices. Consequently, the modified stabilizer is obtained by augmenting S with Z operators acting on the edge qubit along this path matching. The high-level representation is shown on the right of Fig. 3(b), where the modified stabilizer S' is connected to the edge qubits E via the path matching μ .

Third, the independent cycle basis of the graph G corresponds to the gauge qubits introduced during the code surgery. The associated logical operators can dress the logical operators of the original code, thereby potentially reducing the code distance. Therefore, it is necessary to fix this gauge freedom. Let R be a cycle basis of G . For each cycle $C \in R$, we add the stabilizer $B_C = \prod_{e \in C} Z(e)$ to $\tilde{\mathcal{S}}$. An example and its high-level representation are shown in Fig. 3(c), where three cycle checks are added to the deformed code.

We show examples in Figure 4. Figure 4(a) using lattice surgery on the surface code as an example. In this case, the ancilla system corresponds to an additional surface code patch (“Ancilla Patch”), which can be viewed as a graph as discussed in Section 2.2. This ancilla patch is attached to two surface code patches supporting logical operators L_{X1} and L_{X2} , and effectively couples them. From the graph perspective, this corresponds to connecting two logical operators through an intermediate graph structure, which enables their joint measurement using only local interactions. As a result, the product $L_{X1}L_{X2}$ is promoted to a stabilizer of the deformed code and can be measured via local checks. This demonstrates that lattice surgery is a special case of the general code surgery framework.

Code communications. The same principle extends naturally to communication between different codes. To measure a joint logical operator L_1L_2 between two codes \mathcal{Q}_1 and \mathcal{Q}_2 , we first construct separate ancilla graphs for each logical

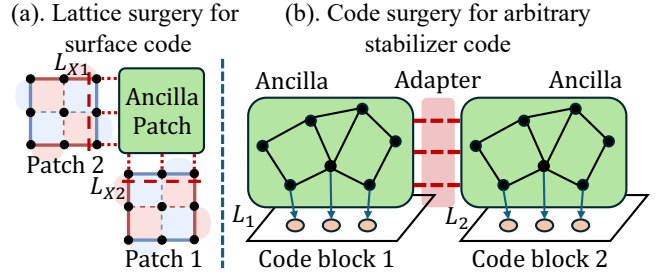


Figure 4. Overview of code surgery construction

operator and then connect them via an *adapter* [33] (or a *bridge* when the codes belong to the same family), which links corresponding ports across the two graphs. The overall procedure is illustrated in Figure 4(b), where two code blocks are connected via an adapter. Each code block is associated with its own ancilla graph, and the adapter links the corresponding ports between them. From the graph viewpoint, this corresponds to coupling the two logical operators through the adapter edges, resulting in a deformed code in which L_1L_2 is promoted to a measurable operator, enabling joint logical measurement and state transfer between the two codes. As in the single-code setting, the efficiency of this process depends critically on the structure of the underlying ancilla graphs, motivating the need for optimized graph construction.

3 Motivation and Problem Formulation

Code surgery constructs an ancilla system to enable fault-tolerant measurement of logical operators. While cross-code communication additionally requires connecting two ancilla systems via an adapter (or bridge), the size of the adapter is exactly the code distance d , and is therefore typically much smaller than the ancilla systems themselves [33]. Therefore, in this work, we focus on optimizing the construction of the ancilla system, which dominates the overall resource cost.

As discussed in Section 2.2, the ancilla system can be represented as a graph whose structure determines both correctness and resource cost. This perspective allows us to formulate code surgery synthesis as a graph construction problem. Given a stabilizer code \mathcal{Q} and a logical operator L , the code design objective is to construct an ancilla system (with additional qubits and new checks) such that:

- the resulting deformed code preserves fault tolerance (e.g., code distance),
- the ancilla system uses minimal physical resources (numbers of qubits and checks),
- the construction satisfies the low-density parity-check (LDPC) constraints.

Importantly, the objectives of code design can be translated into structural properties of the graph [22, 35]. In particular, properties such as distance preservation, bounded

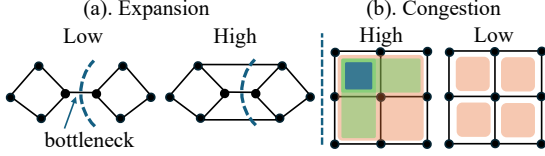


Figure 5. Expansion and congestion

stabilizer weight, and limited qubit participation correspond directly to expansion, graph degree, and cycle congestion in the graph. This translation enables us to reason about code surgery through graph properties.

3.1 Design Objectives from the Graph Perspective

Here, we provide an intuitive overview of the key graph properties used in this paper. Formal definitions of these concepts, along with the baseline graph construction algorithm [22, 35], are in Appendix A.1.

Expansion. The graph must have sufficient connectivity, meaning it cannot be separated into two large parts by removing only a small number of edges. As illustrated in Figure 5(a), low-expansion graphs contain bottlenecks where two large regions are connected by only one edge. In contrast, high expansion eliminates such bottlenecks, ensuring that every partition of the graph has a large edge boundary. The expansion property can be quantified by the (relative) Cheeger constant of the graph (see Appendix A.1 for definition). In our construction, we need the relative Cheeger constant to be larger than 1 to theoretically guarantee the preservation of code distance. Intuitively, this ensures that when a logical operator is “pushed” through the vertex checks, its support is mapped to the edge boundary of the corresponding vertex set; requiring the relative Cheeger constant to be at least 1 guarantees that this boundary is no smaller than the original support, preventing any shrinkage and thus preserving the code distance.

Congestion. The cycle structure is captured by the notion of congestion, which measures how much cycles in a chosen cycle basis overlap on edges. As illustrated in Figure 5(b), in the left example, the cycles (highlighted in green, blue, and orange) heavily overlap in the same region, with some edges shared by multiple cycles (e.g., up to four), resulting in high congestion. In contrast, in the right example, the cycles are more evenly distributed, and each edge is contained in only a constant number of cycles (e.g., at most two), leading to low congestion. Our goal is therefore to construct a cycle basis with low congestion, as congestion translates to qubit degree. Intuitively, since each cycle corresponds to a check, heavy overlap among cycles implies that an edge (and thus its corresponding qubit) participates in many such checks, leading to a higher degree.

Degree Constraints. The graph must satisfy bounded-degree conditions: each vertex has constant degree, and the cycles in the chosen cycle basis have constant length.

3.2 Design Challenges

These objectives are inherently coupled and often conflicting. Increasing expansion typically requires adding edges, which improves connectivity but also raises resource usage and may lead to higher congestion due to more overlapping cycles. At the same time, enforcing strict degree constraints limits the graph structure, potentially reducing expansion or introducing additional overhead. As a result, constructing an efficient graph requires carefully balancing these objectives rather than optimizing them independently.

3.3 Problem Statement

We formulate the code surgery synthesis problem as follows:

Given a stabilizer code Q and a logical operator L , construct an ancilla graph G that satisfies expansion, congestion, and degree constraints while minimizing the total resource overhead.

This formulation highlights that code surgery is fundamentally a *multi-objective graph optimization problem*. Existing constructions [22, 35] prioritize worst-case guarantees and treat these objectives in a fixed pipeline, introducing significant redundancy in practice. In contrast, our approach treats these objectives jointly and dynamically, enabling more efficient constructions tailored to the input code structure.

4 Optimizing Expander Construction via Conditioned Randomization

In Section 3, we formulated code surgery synthesis as a graph construction problem, where one of the key objectives is to construct an ancilla graph that achieves sufficient expansion, namely *expander*, while minimizing resource overhead.

In existing constructions, the graph is built in multiple stages. As illustrated in left of Figure 6, the construction first introduces a *path-matching graph* (see Section 2.3), which

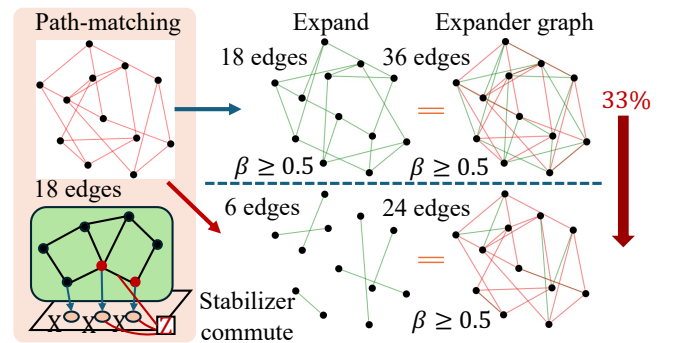


Figure 6. Expand on path-matching graph. β : Cheeger constant.

arises from enforcing commutation between the original stabilizers and the newly introduced vertex checks. This initial graph already contains a nontrivial amount of connectivity, as logical operators are frequently checked by the opposite stabilizers.

However, prior approaches treat this graph merely as an intermediate object and construct a constant-degree graph (expander) independently on top of it (Figure 6, top). This ignores the connectivity already present in the path-matching graph, yielding redundant edges and unnecessary overhead.

4.1 Conditioned Expander Construction

We propose a low-overhead structure-aware expander construction algorithm that leverages the existing path-matching graph to achieve the expansion requirement. Instead of constructing a full expander independently, our approach progressively augments the graph by adding edges in a randomized manner while continuously monitoring its expansion. As illustrated at the bottom of Figure 6, this process gradually improves connectivity using only a small number of additional edges until the desired expansion is achieved.

We present our construction in Algorithm 1, which leverages the uniform random graph generation algorithm of [31]. Their approach generates d -regular graphs on n vertices approximately uniformly at random.

Given a path-matching graph G_0 , our goal is to construct a graph G whose Cheeger constant exceeds a prescribed threshold β , while minimizing the number of added edges. In our construction, β is chosen to be a constant smaller than 1, as enforcing $\beta = 1$ directly would lead to excessive congestion. The procedure for boosting the expansion to the desired level ($\beta > 1$) will be addressed in the Section 5.

Key Idea. Instead of constructing an expander independently, we *condition* the construction on the existing path-matching graph G_0 . This allows us to reuse existing edges and avoid redundant connectivity. Our construction has two phases.

Phase 1: Regularization to Maximum Degree. We first compute the maximum degree Δ over all vertices. Let $\deg_G(v)$ denote the degree of vertex v . We then iteratively add edges between vertices with remaining degree capacity.

At each step, we select a pair $\{u, v\}$ with $\deg_G(u) < \Delta$ and $\deg_G(v) < \Delta$, with probability proportional to $(\Delta - \deg_G(u))(\Delta - \deg_G(v))$, and add the edge to G .

After each addition, we evaluate the expansion of the graph. Directly computing expansion (i.e., calculating the exact Cheeger constant) is computationally intractable [7]. Instead, we use the second smallest eigenvalue λ_2 of the graph Laplacian as a proxy. By Cheeger's inequality,

$$\beta_G \geq \lambda_2/2,$$

so larger λ_2 implies better expansion. We monitor λ_2 during construction and terminate once $\lambda_2 \geq 2\beta$.

Algorithm 1: Conditioned Expander Construction

Input: Path matching graph G_0 , expansion threshold β , maximum number of iterations τ

Output: Graph $G = (V, E)$ with $\lambda_2(G) \geq 2\beta$

Initialization: $G \leftarrow G_0$; $iteration \leftarrow 0$;

Phase 1: Regularization to Maximum Degree;

Compute $\Delta \leftarrow \max_v \deg_G(v)$;

while $\exists v \in V$ such that $\deg_G(v) < \Delta$ **do**

 Define deficit $\Delta(v) \leftarrow \Delta - \deg_G(v)$ for all $v \in V$;

 Let $S = \{\{u, v\} \mid u \neq v, \Delta(u) > 0, \Delta(v) > 0\}$;

if $S = \emptyset$ **then break**;

 Select $\{u, v\} \in S$ with probability proportional to $\Delta(u)\Delta(v)$;

 Add edge $\{u, v\}$ to G ; Compute $\lambda_2(G)$;

if $\lambda_2(G) \geq 2\beta$ **then return** G ;

Phase 2: Degree Augmentation;

while $iteration < \tau$ **do**

$iteration \leftarrow iteration + 1$; Let $U \leftarrow V$;

while $U \neq \emptyset$ **do**

 Let $S = \{\{u, v\} \mid u, v \in U, u \neq v\}$;

if $S = \emptyset$ **then break**;

 Select $\{u, v\} \in S$ uniformly at random;

 Remove u, v from U ;

 Add edge $\{u, v\}$ to G ; Compute $\lambda_2(G)$;

if $\lambda_2(G) \geq 2\beta$ **then return** G ;

Phase 2: Degree Augmentation. If Phase 1 cannot reach the desired expansion, we continue augmenting the graph by adding random 1-regular layers. At each iteration, we generate a random matching and add edges progressively, checking λ_2 after each addition. The process stops as soon as the expansion requirement is satisfied. This two-phase design balances two objectives:

- Phase 1 maximally exploits existing structure,
- Phase 2 ensures expansion when structure alone is insufficient.

In practice, we repeat the randomized construction multiple times and select the smallest resulting graph.

4.2 Sampling Expanders with High Probability

Our expander construction Algorithm 1 randomly samples edges to construct the graph. Here we show that Algorithm 1 produces an expander successfully with high probability. We first define the probability space for our sampling algorithm.

Definition 4.1 (Random Regular Graph Models). *Let $n, r \in \mathbb{N}$ with nr even.*

(1) Simple r -regular graph. *Let $\Omega_{n,r}$ denote the set of all simple r -regular graphs on n labelled vertices, and let $\mathcal{F}_{n,r} =$*

$2^{\Omega_{n,r}}$. Let $\mathbb{U}_{n,r}$ be the uniform distribution over $\Omega_{n,r}$. We define

$$G(n, r) : (\Omega_{n,r}, \mathcal{F}_{n,r}, \mathbb{U}_{n,r}) \rightarrow (\Omega_{n,r}, \mathcal{F}_{n,r})$$

as a random element taking values in $\Omega_{n,r}$, corresponding to a uniformly sampled simple r -regular graph, which can be obtained via the configuration model conditioned on simplicity.

(2) **Special case** ($r = 1$). When $r = 1$, $G(n, 1)$ corresponds to a uniformly random perfect matching on n vertices.

(3) **Loopless multigraph model**. Let $G'(n, r)$ denote the random multigraph generated by the configuration model conditioned on being loopless, while allowing multiple edges. This defines a probability space $(\Omega'_{n,r}, \mathcal{F}'_{n,r}, \mathbb{P}'_{n,r})$.

In this probability space, we can model the sampling process with the following definition.

Definition 4.2 (Union of Random Matchings). Let $n, r \in \mathbb{N}$ with n even. Let $G(n, 1)$ denote a random perfect matching on n vertices with probability space $(\Omega_{n,1}, \mathcal{F}_{n,1}, \mathbb{U}_{n,1})$.

We define the random graph $\mathcal{I}(n, r)$ as the union of r independent samples of $G(n, 1)$: $\mathcal{I}(n, r) = G_1 + G_2 + \dots + G_r$, where $+$ denotes graph union on a common vertex set.

Equivalently, $\mathcal{I}(n, r)$ can be viewed as a random element

$$\mathcal{I}(n, r) : (\Omega_{n,1}^{\otimes r}, \mathcal{F}_{n,1}^{\otimes r}, \mathbb{U}_{n,1}^{\otimes r}) \rightarrow (\Omega'_{n,r}, \mathcal{F}'_{n,r}),$$

where $\Omega'_{n,r}$ denotes the space of loopless multigraphs on n vertices with degree r .

Finally, the following theorem states that our graph construction method samples an expander with high probability.

Theorem 4.1 (Expansion via Reduction to $\mathcal{I}(n, r)$). Let G be the graph produced by Algorithm 1. Then, as $n \rightarrow \infty$, G is an expander with probability $1 - o(1)$.

Proof. We first observe that the graph constructed in Phase 2 in Algorithm 1 can be viewed as a realization of $\mathcal{I}(n, r)$, the union of r independent random perfect matchings on n vertices. Moreover, since adding edges can only increase the expansion, the expansion of G is at least that of $\mathcal{I}(n, r)$. By Corollary 1.4 in [18], $\mathcal{I}(n, r)$ is an expander with probability $1 - o(1)$ as $n \rightarrow \infty$. Therefore, G is also an expander with high probability. \square

Remark 4.1. In certain corner cases (e.g., due to parity constraints), a perfectly d -regular graph may not exist. In such cases, we allow a small deviation from regularity by assigning one vertex a degree higher by one than the others. Since this modification affects only a constant number of vertices, it does not alter the asymptotic expansion guarantees.

5 Balancing Expansion and Congestion

In the previous section, we constructed an expander graph with reduced edge redundancy. However, this construction leaves two important issues unresolved. First, the achieved expansion is bounded by a constant $\beta < 1$, and must be further boosted to meet stronger expansion requirements.

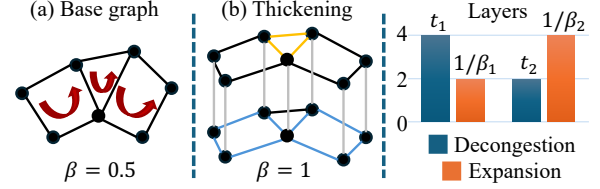


Figure 7. Graph thickening and the trade-off between decongestion and expansion

Second, the resulting graph may admit cycle basis with non-trivial congestion, rather than the desired constant congestion, as cycles can overlap significantly on certain edges.

5.1 Graph Thickening and Its Overhead

Graph thickening provides a mechanism to simultaneously boost expansion and reduce congestion. Starting from a base graph with Cheeger constant β (e.g., $\beta = 0.5$ in Figure 7(a)), it constructs multiple copies of the graph and connects them across layers. By using more edges (i.e., more physical qubits in the synthesized ancilla system), this method increases the relative expansion to $\ell \cdot \beta$ after ℓ layers, while allowing cycles to be distributed across layers (e.g., the blue and yellow cycles in Figure 7(b)), thereby reducing overlap.

To quantify the amount of decongestion required, we partition the cycle basis of the base graph into edge-disjoint groups using a greedy procedure, and let t denote the number of such groups. Intuitively, t captures the number of layers needed to fully separate overlapping cycles. As a result, the total number of layers required by thickening is given by $\ell = \max(t, 1/\beta)$.

However, this introduces a fundamental trade-off as shown in right of Figure 7. A larger β reduces the number of layers required for boosting expansion, but leads to higher congestion and thus requires more layers for decongestion. Conversely, a smaller β simplifies decongestion but increases the number of layers needed to achieve sufficient expansion.

This observation motivates our main technique for this section: instead of fixing β in advance, we dynamically monitor the congestion during the expander construction, and identify a trade-off point at which the layers required for boosting expansion and decongestion are balanced.

5.2 Dynamic Cycle Tracking Algorithm

We again start with a path-matching graph G_0 and apply the Decongestion Lemma (Lemma A.0.2 in [17]) to construct a cycle basis \mathcal{R}_0 for G_0 . We can also calculate a spanning forest T_0 of G_0 .

Since our goal in this section is to monitor how the cycle basis evolves as new edges are added, we introduce a cycle-tracking algorithm (Algorithm 2). Given the current cycle basis \mathcal{R}_i , the spanning forest T_i , and a newly added edge $e_i = (u, v)$, the algorithm outputs an updated cycle basis \mathcal{R}_{i+1} and a new spanning forest T_{i+1} .

Algorithm 2: Dynamic Cycle Basis Maintenance

Input: Cycle basis \mathcal{R}_i , spanning forest T_i , new edge $e_i = (u, v)$
Output: Updated cycle basis \mathcal{R}_{i+1} , spanning forest T_{i+1} , optionally a new cycle basis r_{i+1}
if u and v are not connected in T_i **then**
 $T_{i+1} \leftarrow T_i \cup \{e_i\}; \mathcal{R}_{i+1} \leftarrow \mathcal{R}_i; r_{i+1} \leftarrow \phi;$
else
 Let $P_{T_i}(u, v)$ be the unique path between u and v in T_i ; $r_{i+1} \leftarrow P_{T_i}(u, v) \cup \{e_i\};$
 $\mathcal{R}_{i+1} \leftarrow \mathcal{R}_i \cup \{r_{i+1}\}; T' \leftarrow T_i \cup \{e_i\};$
 Remove an edge from $P_{T_i}(u, v)$ in T' ; $T_{i+1} \leftarrow T';$
return $(\mathcal{R}_{i+1}, T_{i+1}, r_{i+1});$

Algorithm 2 maintains the cycle basis dynamically. If u and v lie in different connected components of T_i , the edge e_i is added to the forest and the cycle basis remains unchanged. Otherwise, e_i induces a unique fundamental cycle formed by the path between u and v in T_i , which is appended to the cycle basis. To preserve the forest structure, an edge on the corresponding path is removed, optionally using a randomized or load-aware rule [34].

Maintaining Low Congestion. We now analyze the congestion of the cycle basis constructed by Algorithm 2, and present the following theorem.

Theorem 5.1 (Low Congestion under Short Paths). *Let G be a graph with n vertices and m edges. If the spanning forest maintains diameter $O(\log n)$ throughout Algorithm 2, then the resulting cycle basis has congestion $O(\log n \cdot \log m)$ with probability at least $1/2$.*

Proof. Under the assumption that each path has length at most $O(\log n)$, the Decongestion Lemma implies that for any fixed edge e , the probability that it remains unremoved after w cycles is at most

$$(1 - \Omega(1/\log n))^w.$$

For $w = O(\log n \cdot \log m)$, this probability can be made at most $1/(2m)$.

Applying a union bound over all edges, we conclude that with probability at least $1/2$, no edge participates in more than $O(\log n \cdot \log m)$ cycles. This establishes the desired congestion bound. \square

The above theorem relies on the assumption that the spanning forest maintains short paths of length $O(\log n)$. However, this condition may not hold in general. In the worst case, an arbitrary spanning forest may contain paths of length $O(n)$, which invalidates the low-congestion guarantee.

In our setting, the underlying graph is an expander, which has diameter $O(\log n)$ [23]. By recomputing the spanning forest a constant number of times (e.g., via BFS), we ensure that the spanning forest periodically returns to a low-diameter

Algorithm 3: Dynamic Greedy Cycle Partition

Input: Existing partition $\mathcal{R}_i = \bigcup_{k=1}^{t_i} P_k$, new cycle r_{i+1}
Output: Updated partition $\mathcal{R}_{i+1} = \bigcup_{k=1}^{t_{i+1}} P_k$, decongestion layer t_{i+1}
for $k \leftarrow 1$ **to** t_i **do**
 if r_i does not overlap with any cycle in P_k **then**
 $P_k \leftarrow P_k \cup \{r_{i+1}\};$
 return $\bigcup_{k=1}^{t_i} P_k, t_i;$
 $P_{t_{i+1}} \leftarrow \{r_{i+1}\};$
return $\bigcup_{k=1}^{t_{i+1}} P_k, t_i + 1;$

structure. Nevertheless, between such resets, the spanning forest may drift due to edge updates. In the worst case, it may resemble a random-like forest with diameter $O(\sqrt{n})$ [1], leading to a degraded congestion bound of $O(\sqrt{n} \cdot \log m)$.

Independence of the Cycle Basis. Since the spanning tree is dynamically modified (e.g., due to resets), it is not immediate that the cycles produced by Algorithm 2 still form a valid cycle basis. In particular, we need to ensure that these updates do not destroy linear independence.

Theorem 5.2 (Independence of the Constructed Cycle Basis). *Let r_1, \dots, r_k denote the cycle basis obtained by applying the Decongestion Lemma to the path-matching graph, and let r_{k+1}, \dots, r_l be the additional cycles generated by Algorithm 2 during the expander construction process. Then the set $\{r_1, \dots, r_l\}$ is linearly independent.*

Proof. Consider a linear combination

$$a_1 r_1 + \dots + a_k r_k + a_{k+1} r_{k+1} + \dots + a_l r_l = 0.$$

We show that all coefficients must be zero.

For each $i > k$, the cycle r_i is formed using a newly added edge that does not appear in any previously constructed cycles. In particular, the most recently added cycle r_l contains an edge that appears uniquely in r_l , implying that $a_l = 0$.

Applying the same argument inductively, we obtain $a_{l-1} = \dots = a_{k+1} = 0$. Since r_1, \dots, r_k form a basis by construction, it follows that $a_1 = \dots = a_k = 0$. This completes the proof. \square

5.3 Dynamically Compute Decongestion Layer

After updating the cycle basis \mathcal{R}_{i+1} , we compute the layer t_{i+1} for decongestion at this step. We attempt to place the new cycles into existing partition groups without overlap; if not possible, we create a new group (see Algorithm 3).

Thickening Layer Upper Bound. We calculate the upper bound on the decongestion layer t by reducing our Dynamic Greedy Cycle Partition to a known Greedy Partition Algorithm (Corollary 15 in [22]). This known Greedy Partition Algorithm provides an upper bound on the thickening layer t , which is given by the product of the average cycle length and the cycle basis congestion. We show that

recursively applying our progressive partition procedure is functionally equivalent when combined with our congestion-aware expander construction (see Algorithm 4 later in Section 5.4).

Lemma 5.1. *The progressive partition procedure (Algorithm 3) produces the same partition as the Greedy Partition algorithm (see Corollary 15 in [22]) applied to the full set of cycles.*

Proof. We prove the claim by induction on the number of cycles. Let the cycles be ordered as $\mathcal{R} = \{r_1, \dots, r_t\}$.

Base case. For $l = 1$, both algorithms place r_1 into the first group, and hence the resulting partitions are identical.

Inductive step. Assume processing $t - 1$ cycles, both algorithms produce the same partition $\{P_1, \dots, P_k\}$. Now we consider processing t cycles.

In the Greedy Partition algorithm, observe that r_t is always the last cycle to be checked within each partition group, and therefore does not affect the placement of any preceding cycles. Therefore, its placement can be viewed as occurring after all operations on the first $t - 1$ cycles have been completed. By the induction hypothesis, the partition formed by the first $t - 1$ cycles is identical to that produced by our incremental algorithm.

Thus, after inserting r_t , the partitions produced by both algorithms remain the same. By induction, the two algorithms produce identical partitions for all cycles. \square

As a result, our method inherits the same upper bound $O((\log(n))^3)$ on the decongestion layer t per Lemma 5.1. We highlight that this equivalence is non-trivial. A naive approach would recompute the greedy partition after each insertion, incurring significant overhead. In contrast, our method updates the partition incrementally by only checking the newly added cycle against existing groups, naturally accommodating our dynamic cycle tracking algorithm and reducing the complexity by a factor of $O(n)$ without changing the result.

5.4 Finding Expansion–Congestion Balance Point

Using the procedure for tracking the decongestion layer after each edge insertion, we propose Algorithm 4 that automatically identifies the expansion-congestion balancing point during the expander construction. Leveraging the two techniques above, it augments Algorithm 1 by, after adding each edge, checking the number of layers required for boosting expansion, $\lceil 2/\lambda_2(G_i) \rceil$, and comparing it with the number of layers required for decongestion, t_i . Since the former is monotonically decreasing while the latter is monotonically increasing, we terminate once the latter exceeds the former. No physical resources are wasted on an unbalanced construction.

Remark 5.1. *An alternative approach is to recompute a cycle basis using the Decongestion Lemma after each edge insertion,*

Algorithm 4: Congestion–Aware Expander Construction

Input: Path-matching graph G_0 , BFS tree resetting step τ , maximum number of iterations τ

Output: Graph G with balanced expansion and congestion layers

Initialization: $G \leftarrow G_0$; $step \leftarrow 0$; $iteration \leftarrow 0$;
Compute $\mathcal{R}_0 \leftarrow$ Decongestion Lemma applied to G ;
Compute partition $\mathcal{R}_0 = \bigcup_{k=1}^{t_0} P_k$ using Greedy Partition;

Compute $T_0 \leftarrow$ BFS forest of G ;

Phase 1: Regularization to Maximum Degree;

Compute $\Delta \leftarrow \max_v \deg_G(v)$;

while $\exists v \in V$ such that $\deg_G(v) < \Delta$ **do**

Define deficit $\Delta(v) \leftarrow \Delta - \deg_G(v)$ for all $v \in V$;

Let $S = \{\{u, v\} \mid u \neq v, \Delta(u) > 0, \Delta(v) > 0\}$;

if $S = \emptyset$ **then break**;

Select $\{u, v\} \in S$ with probability proportional to $\Delta(u)\Delta(v)$, add edge $\{u, v\}$ to G ;

Compute $\lambda_2(G)$;

$(\mathcal{R}_{i+1}, T_{i+1}, r_{i+1}) \leftarrow$ Algorithm 2($\mathcal{R}_i, T_i, (u, v)$);

$\mathcal{R}_{i+1} = \bigcup_{k=1}^{t_{i+1}} P_k$, $t_{i+1} \leftarrow$ Algorithm 3(\mathcal{R}_i, r_{i+1});

if $t_{i+1} \geq \lceil 2/\lambda_2(G) \rceil$ **then**

\lfloor **return** G ;

$step \leftarrow step + 1$;

if $step \bmod \tau = 0$ **then**

\lfloor $T_{i+1} \leftarrow$ BFS forest of G ;

Phase 2: Degree Augmentation;

while $iteration < \tau$ **do**

$iteration \leftarrow iteration + 1$; Let $U \leftarrow V$;

while $U \neq \emptyset$ **do**

Let $S = \{\{u, v\} \mid u, v \in U, u \neq v\}$;

if $S = \emptyset$ **then break**;

Select $\{u, v\} \in S$ uniformly at random;

Remove u, v from U , add edge $\{u, v\}$ to G ;

Compute $\lambda_2(G)$;

$(\mathcal{R}_{i+1}, T_{i+1}, r_{i+1}) \leftarrow$ Algorithm 2($\mathcal{R}_i, T_i, (u, v)$);

$\mathcal{R}_{i+1} = \bigcup_{k=1}^{t_{i+1}} P_k$, $t_{i+1} \leftarrow$ Algorithm 3(\mathcal{R}_i, r_{i+1});

if $t_{i+1} \geq \lceil 2/\lambda_2(G) \rceil$ **then**

\lfloor **return** G ;

$step \leftarrow step + 1$;

if $step \bmod \tau = 0$ **then**

\lfloor $T_{i+1} \leftarrow$ BFS tree of G ;

followed by running greedy partition algorithm. While the Decongestion Lemma admits a polynomial-time implementation and provides strong theoretical guarantees on low congestion,

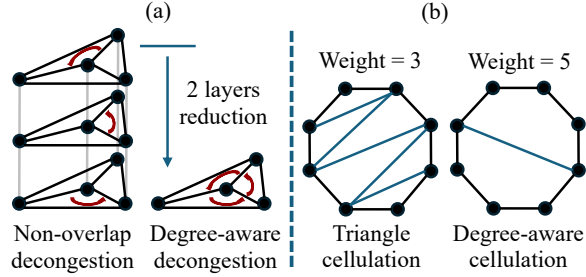


Figure 8. Degree-aware graph optimization

this approach incurs significantly higher compilation time compared to our dynamic cycle basis maintenance algorithm in practice. In particular, it requires recomputing the entire cycle basis at each step, whereas our method only performs progressive updates. The compilation quality of two approaches are similar in practice, we provide both implementations in our software.

6 Incorporating Degree Constraints

Finally, we incorporate the LDPC constraints to achieve more resource-efficient decongestion and cellulation. In Figure 8(a), allowing controlled overlap under degree constraints enables more flexible cycle placement, reducing the number of layers compared to strictly non-overlapping decongestion. In Figure 8(b), degree-aware cellulation replaces uniform triangulation with higher-degree faces, reducing the number of checks (e.g., from 6 to 2) while respecting the degree bound (5 in this example). These observations motivate incorporating degree constraints into both decongestion and cellulation.

6.1 Degree-Aware Cycle Basis Partition

We first incorporate degree constraints into cycle partitioning, which is central to the decongestion process. Observe that two types of cycle partitioning are used in Algorithm 4: a static partition performed after constructing the path-matching graph, and a dynamic partition (Algorithm 3) applied each time a new edge is sampled, generating a new cycle that is then assigned to a partition group.

To this end, we introduce a tracker for edge load within each cycle group P_k in the partition $\mathcal{R}_i = \bigcup_{k=1}^{t_i} P_k$. This tracker records the number of cycles in which each edge participates within a given group. When attempting to place a new cycle into a group P_k , we examine each edge in the cycle and check whether its load would exceed a prescribed maximum d_q qubit degree determined by the LDPC degree constraints. If all edges satisfy this condition, the cycle is assigned to P_k ; otherwise, it is considered for the next group. We present this method in Algorithm 5.

6.2 Degree-Aware Cellulation

We now incorporate check degree constraints into the cellulation process. In the theoretical construction [22, 35], cycles

Algorithm 5: Degree-Constrained Cycle Partition

Input: Existing partition $\mathcal{R}_i = \bigcup_{k=1}^{t_i} P_k$, new cycle r_{i+1} , load trackers $\{\ell_k\}_{k=1}^{t_i}$, max degree load d_q

Output: Updated partition $\mathcal{R}_{i+1} = \bigcup_{k=1}^{t_{i+1}} P_k$, updated trackers $\{\ell_k\}_{k=1}^{t_{i+1}}$, decongestion layer t_{i+1}

for $k \leftarrow 1$ **to** t_i **do**

if $\forall e \in r_{i+1}, \ell_k(e) + 1 \leq d_q$ **then**

$P_k \leftarrow P_k \cup \{r_{i+1}\};$

foreach $e \in r_{i+1}$ **do** $\ell_k(e) \leftarrow \ell_k(e) + 1;$

return $\bigcup_{k=1}^{t_i} P_k, \{\ell_k\}_{k=1}^{t_i}, t_i;$

$P_{t_{i+1}} \leftarrow \{r_{i+1}\};$ Define a new tracker $\ell_{t_{i+1}};$

foreach $e \in r_{i+1}$ **do** $\ell_{t_{i+1}}(e) \leftarrow 1;$

return $\bigcup_{k=1}^{t_{i+1}} P_k, \{\ell_k\}_{k=1}^{t_{i+1}}, t_i + 1;$

Table 1. Benchmark information

Benchmark	BB code	HP code	QT code
[[n, k, d]]	[[72, 12, 6]]	[[450, 32, 8]]	[[81, 13, 4]]
	[[90, 8, 10]]	[[882, 50, 10]]	[[90, 15, 4]]
	[[108, 8, 10]]	[[882, 98, 8]]	[[117, 17, 4]]
	[[144, 12, 12]]	[[1800, 72, 14]]	[[126, 19, 4]]
	[[288, 12, 18]]	[[1922, 200, 12]]	[[135, 23, 4]]
Benchmark	Surface code		Color code
[[n, k, d]]	[[25, 1, 5]]	[[441, 1, 21]]	[[19, 1, 5]]
	[[49, 1, 7]]	[[1681, 1, 41]]	[[37, 1, 7]]
	[[81, 1, 9]]	[[3721, 1, 61]]	[[61, 1, 9]]
	[[121, 1, 11]]	[[6561, 1, 81]]	[[91, 1, 11]]
	[[169, 1, 13]]	[[10201, 1, 101]]	[[127, 1, 13]]

are cellulated into triangles using a zigzag procedure, ensuring that each cycle check acts on exactly three qubits.

To better match check degree constraints, we generalize this construction by replacing triangular cellulation with d_c -gon cellulation, where d_c denotes the maximum allowed check degree. The goal is to ensure that each check acts on at most d_c qubits. Our construction follows the zigzag pattern as in the triangular case. Given a cycle $C = (v_1, v_2, \dots, v_\ell)$, we introduce auxiliary edges in a structured zigzag manner to decompose the cycle into a collection of smaller cycles, each involving at most d_c vertices. Instead of forming triangles by connecting vertices in a stepwise zigzag fashion, we extend the pattern to span d_c vertices before closing each face. This zigzag d_c -gon cellulation ensures that each resulting cycle check has weight at most d_c , as required by the LDPC constraints. Thus, by extending the same zigzag pattern from the triangular case, we can directly control the maximum check weight without altering the overall construction.

Table 2. Resources to implement the ancilla system and the compiler runtime

BB code	[[72, 12, 6]] (89%)			[[90, 8, 10]] (88%)			[[108, 8, 10]] (88%)			[[144, 12, 12]] (90%)			[[288, 12, 18]] (88%)		
	Size	Deg	Time	Size	Deg	Time	Size	Deg	Time	Size	Deg	Time	Size	Deg	Time
CKBB	84/81	7/7	0.24	240/235	7/7	0.24	348/342	7/7	0.24	348/342	7/7	0.24	792/783	7/7	0.24
Gauge	90/91	8/8	0.05	157/158	8/10	0.06	185/186	8/9	0.07	239/240	8/10	0.07	362/363	8/11	0.09
Exp-Opt	42/43	7/7	0.06	100/101	7/7	0.07	153/154	7/7	0.08	122/123	7/8	0.20	234/235	7/8	0.40
Cong-Opt	42/43	7/7	0.20	100/101	7/7	0.29	123/124	7/7	0.35	89/90	7/7	0.41	184/185	7/7	0.63
Full-Opt	9/10	7/7	0.21	19/20	7/7	0.57	23/24	7/7	0.81	24/25	7/8	0.87	45/46	9/9	1.80
HP code	[[450, 32, 8]] (89%)			[[882, 50, 10]] (88%)			[[882, 98, 8]] (90%)			[[1800, 72, 14]] (88%)			[[1922, 200, 12]] (90%)		
CKBB	152/148	7/7	0.24	240/235	7/7	0.24	225/217	9/9	0.24	600/589	9/9	0.24	432/419	11/11	0.25
Gauge	122/123	8/10	0.06	155/156	8/9	0.07	174/175	10/12	0.07	301/302	10/12	0.11	302/303	11/13	0.10
Exp-Opt	56/57	7/7	0.07	98/99	7/7	0.08	104/105	9/10	0.08	180/181	9/10	0.11	206/207	11/12	0.11
Cong-Opt	56/57	7/7	0.24	71/72	7/7	0.29	78/79	9/10	0.34	136/137	9/10	0.62	164/165	11/12	0.60
Full-Opt	14/15	7/7	0.41	19/20	7/7	0.63	18/19	9/10	0.33	35/36	9/10	1.15	30/31	11/12	0.59
QT code	[[81, 13, 4]] (86%)			[[90, 15, 4]] (86%)			[[117, 17, 4]] (85%)			[[126, 19, 4]] (80%)			[[135, 23, 4]] (83%)		
CKBB	28/28	7/7	0.24	28/28	7/7	0.24	78/76	7/7	0.23	220/217	7/7	0.24	312/309	7/7	0.24
Gauge	38/39	7/7	0.05	38/39	7/7	0.05	66/67	8/10	0.05	109/110	8/10	0.06	171/172	8/9	0.07
Exp-Opt	21/22	6/7	0.05	21/22	6/7	0.05	40/41	7/7	0.06	71/72	7/7	0.12	148/149	7/7	0.26
Cong-Opt	5/6	6/7	0.14	5/6	6/7	0.14	40/41	7/7	0.18	73/74	7/7	0.29	123/124	7/7	0.40
Full-Opt	4/5	6/7	0.14	4/5	6/7	0.14	10/11	7/7	0.30	22/23	8/7	0.71	29/30	8/7	0.97
Surface code	[[25, 1, 5]] (87%)			[[49, 1, 7]] (87%)			[[81, 1, 9]] (86%)			[[121, 1, 11]] (84%)			[[169, 1, 13]] (87%)		
CKBB	84/85	5/5	0.24	84/85	5/5	0.24	220/221	5/5	0.24	312/313	5/5	0.24	684/685	5/5	0.24
Gauge	102/103	8/9	0.06	102/103	8/9	0.06	165/166	8/9	0.07	200/201	8/10	0.07	381/382	8/10	0.09
Exp-Opt	39/40	5/6	0.10	39/40	5/6	0.10	76/77	5/7	0.36	90/91	5/7	0.48	248/249	5/7	0.94
Cong-Opt	47/48	5/7	0.28	47/48	5/7	0.28	76/77	5/7	0.47	124/125	5/7	0.56	243/244	5/7	0.89
Full-Opt	11/12	6/7	0.41	11/12	6/7	0.42	23/24	7/7	0.95	32/33	8/8	1.22	50/51	10/9	2.18
Color code	[[19, 1, 5]] (83%)			[[37, 1, 7]] (87%)			[[61, 1, 9]] (87%)			[[91, 1, 11]] (86%)			[[127, 1, 13]] (88%)		
CKBB	40/41	7/7	0.24	84/85	7/7	0.24	144/145	7/7	0.24	220/221	7/7	0.24	312/313	7/7	0.24
Gauge	53/54	8/8	0.05	102/103	8/9	0.06	137/138	8/10	0.06	164/165	8/9	0.07	254/255	8/10	0.07
Exp-Opt	27/28	6/7	0.09	39/40	6/7	0.10	59/60	6/7	0.26	101/102	6/7	0.35	91/92	6/7	0.47
Cong-Opt	20/21	6/7	0.20	47/48	6/7	0.28	64/65	6/7	0.38	76/77	6/7	0.47	124/125	6/7	0.56
Full-Opt	7/8	6/7	0.26	11/12	6/7	0.41	18/19	7/7	0.67	23/24	7/7	0.91	30/31	8/7	1.22

7 Evaluation

In this section, we evaluate GeneCS by comparing it against state-of-the-art baselines, analyzing the impact of each optimization step, examining code performance under noise, and assessing scalability.

7.1 Experiments Setup.

Baselines. Our baseline code surgery schemes include state-of-the-art the CKBB [8] scheme, and a protocol based on gauging logical operators [22, 35] (denoted as Gauge).

Experimental Configurations. To illustrate the effect of each optimization step, we consider three configurations: (1) Exp-Opt, which enables the conditioned expander construction process introduced in Section 4; (2) Cong-Opt, which incorporates the technique for balancing expansion and congestion during graph construction (Section 5); and (3) Full-Opt, which further incorporates LDPC qubit and check degree constraints into the construction (Section 6).

Benchmarks. We evaluate GeneCS on a variety of QEC code families of different sizes, with detailed information

summarized in Table 1. Here, BB denotes Bivariate Bicycle codes, HP denotes Hypergraph Product codes, and QT denotes Quantum Tanner codes. For each code, we report n (number of physical qubits), k (number of logical qubits), and d (code distance). HP codes are obtained from [2], and QT codes are generated randomly following [30]. For QT codes, we compute the code distance via integer programming [36].

Metrics. We evaluate performance using the following metrics: (a) **Qubit/Check count** (denoted as **Size**): The number of ancillary qubits and checks used in constructing the code surgery system. (b) **Qubit/Check degree** (denoted as **Deg**): The maximum degree of qubit and check in the deformed code system. (c) **Logical error rate**: The simulated logical error rate of the deformed code. (d) **Time**: The CPU time (in second) required to generate the code surgery system.

Implementation. We implement GeneCS in Python. All experiments are conducted on a server with a 2.4 GHz CPU and 0.75 TB of memory. In the graph construction, we perform 100 sampling trials and select the smallest graph (as

described at the end of Section 4.1). For the Gauge baseline, we set the expansion threshold to $\beta = 0.34$, and pick the degree of regular expander as 3. Since the maximum qubit and check degrees in our benchmark codes are 10, we set the degree upper bound of the deformed code to 12. We incorporate the load-aware rule [34] into the cycle basis construction process for both the Gauge baseline and GeneCS.

7.2 Overall Result

We first evaluate the ancilla overhead required for measuring a single logical operator via Code Surgery. We report results for logical X operators, while the results for Z operators are similar. This operation constitutes a fundamental building block of the cross-code logical operations described in Section 7.3. The results are shown in Table 2, where for **Size**, the left (right) entry denotes the number of qubits (checks) for the ancilla system, and for **Deg**, the left (right) entry denotes the maximum qubit (check) degree.

Compared with the smallest code surgery system size achieved by the baseline compilers (CKBB and Gauge), the best results produced by GeneCS achieve an average reduction of 86.7% in the number of ancillary qubits and 85.8% in the number of ancillary checks. We also report the compilation time, in Table 2. All compilations complete within a few seconds. Detailed reduction results for each benchmark are provided in the table alongside their corresponding code instances.

We further analyze the contribution of each optimization technique. The expander optimization (Exp-Opt) achieves a reduction of 41.0% in qubit count and 40.3% in check count. Building on this, the congestion–expansion balancing technique (Cong-Opt) provides an additional reduction of 8.1% for both qubits and checks. Finally, by incorporating degree constraints, we obtain a further reduction of 37.6% in qubit count and 37.4% in check count.

Comparison with best-known results for specific code instances. We compare our constructions with ad-hoc solutions obtained via integer programming [35]. For BB codes $[[144, 12, 12]]$ and $[[288, 12, 18]]$, the best-known ancillary sizes are 22/19 and 34/31 (qubits/checks), with qubit and check degrees both equal to 7. In comparison, GeneCS produces 24/25 and 45/46, with degrees 7/8 and 9/9, respectively. Despite using a general and scalable synthesis framework, our results remain close to these optimized solutions, demonstrating competitive practical resource efficiency.

7.3 Cross-Code Communication

We evaluate the ancillary overhead of measuring joint logical operators between codes. We report results for $X \otimes X$ operators, while other Pauli combinations show similar behavior. We select codes with similar distances from Table 2 and connect them using the bridge/adaptor constructions [33].

First, we evaluate the code surgery system overhead of measuring joint logical operators between good QLDPC

codes and topological codes with comparable distances (row 1&2 in Table 3). GeneCS can accommodate codes with very different distances, but such a configuration is unlikely to be useful in practice because the overall fault tolerance is determined by the lower distance of the two codes being connected. We consider BB, HP, and QT codes combined with surface and color codes. Compared with the baseline compiler (Gauge), our optimized approach (Full-Opt) achieves a reduction of approximately 85% in both ancillary qubit and check counts across all configurations, demonstrating its effectiveness in minimizing the resource cost of cross-family logical operations.

We further evaluate the communication overhead between good QLDPC codes (row 3 in Table 3), considering both homogeneous (e.g., BB+BB, HP+HP, QT+QT) and heterogeneous (e.g., BB+HP) configurations. Cross-family settings involving QT codes are omitted due to their relatively small distance in our benchmark. Compared with the baseline (Gauge), our optimized construction (Full-Opt) achieves a reduction of approximately 86% in both ancillary qubit and check counts across all configurations, demonstrating its effectiveness in enabling resource-efficient logical communication within and across good QLDPC codes.

In addition, for each BB code, we consider two identical code patches and perform a joint measurement of all logical X operators across both patches (row 4 in Table 3). The total number of logical operators measured ranges from 16 to 24. Despite this large number of simultaneously extracted observables, the ancilla size compiled by GeneCS scales very favorably, requiring on average only 1.8 \times the original code size. This represents an average 83% reduction compared to the baseline approach. Our results therefore demonstrate that joint logical operator extraction can be performed with remarkably low overhead, even in the high-rate, multi-logical-qubit setting.

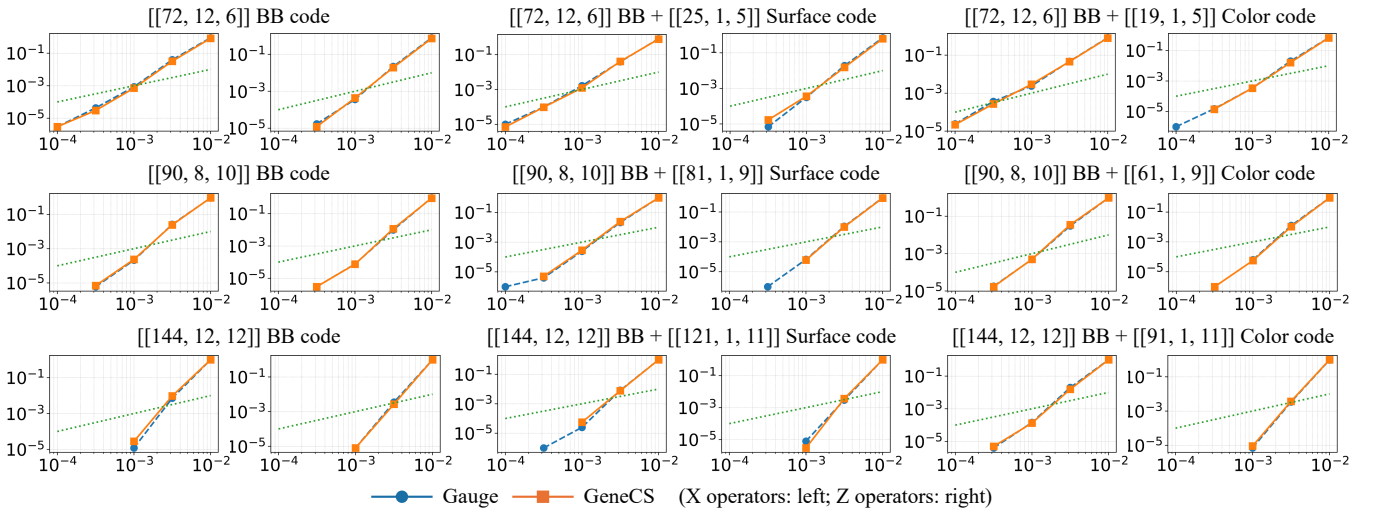
Remark 7.1. *The qubit/check degree constraint is enforced only during the construction of the ancilla graph. In the cross-code communication stage, additional degree may be introduced by the adaptor. However, this increase incurs only a constant overhead, as established in theory [33]. Importantly, such cases can be mitigated via standard post-processing techniques. For example, edges with high congestion can be duplicated to redistribute load and halve the effective edge degree. Likewise, high-degree check nodes can be decomposed using Bell pairs, thereby halving their effective degree. We leave such post-processing techniques for future work.*

7.4 Logical Error Rate Simulation

We simulate the logical error rates of the deformed codes under a circuit-level depolarizing noise model, in which each single/two-qubit gate is followed by an independent depolarizing channel. As shown in Figure 9, each data point is estimated from 10^6 samples; missing points indicate that no

Table 3. Resources to implementation communication between codes with close distances

Code config	BB $[[72, 12, 6]]$ + Surface $[[25, 1, 5]]$			BB $[[90, 8, 10]]$ + Surface $[[81, 1, 9]]$			BB $[[144, 12, 12]]$ + Surface $[[121, 1, 11]]$			HP $[[1922, 200, 12]]$ + Surface $[[121, 1, 11]]$			QT $[[135, 23, 4]]$ + Surface $[[25, 1, 5]]$		
	Size	Deg	Time	Size	Deg	Time	Size	Deg	Time	Size	Deg	Time	Size	Deg	Time
Gauge	197/199	8/9	0.11	331/333	8/11	0.14	450/452	8/11	0.15	513/515	11/14	0.18	277/279	8/10	0.13
Full-Opt	25/27	7/7	0.62	51/53	9/9	1.51	67/69	10/9	2.07	73/75	11/12	1.82	44/46	9/8	1.38
Code config	BB $[[72, 12, 6]]$ + Color $[[19, 1, 5]]$			BB $[[90, 8, 10]]$ + Color $[[61, 1, 9]]$			BB $[[144, 12, 12]]$ + Color $[[91, 1, 11]]$			HP $[[1922, 200, 12]]$ + Color $[[91, 1, 11]]$			QT $[[135, 23, 4]]$ + Color $[[19, 1, 5]]$		
	Size	Deg	Time	Size	Deg	Time	Size	Deg	Time	Size	Deg	Time	Size	Deg	Time
Gauge	148/150	8/9	0.11	303/305	8/11	0.13	414/416	8/11	0.14	477/479	11/14	0.18	228/230	8/10	0.12
Full-Opt	21/23	8/7	0.47	45/47	9/8	1.22	58/60	9/8	1.78	64/66	11/12	1.51	40/42	9/8	1.22
Code config	BB $[[144, 12, 12]]$ + BB $[[144, 12, 12]]$			HP $[[1922, 200, 12]]$ + HP $[[1922, 200, 12]]$			QT $[[135, 23, 4]]$ + QT $[[135, 23, 4]]$			BB $[[90, 8, 10]]$ + HP $[[882, 50, 10]]$			BB $[[144, 12, 12]]$ + HP $[[1922, 200, 12]]$		
	Size	Deg	Time	Size	Deg	Time	Size	Deg	Time	Size	Deg	Time	Size	Deg	Time
Gauge	490/492	8/11	0.15	616/618	11/14	0.21	346/348	8/10	0.14	322/324	8/11	0.14	553/555	11/14	0.18
Full-Opt	60/62	9/8	1.74	72/74	11/12	1.18	58/60	9/10	1.94	48/50	9/8	1.17	66/68	11/12	1.48
Code config	BB $[[72, 12, 6]] \times 2$ 24 joint X logicals			BB $[[90, 8, 10]] \times 2$ 16 joint X logicals			BB $[[108, 8, 10]] \times 2$ 16 joint X logicals			BB $[[144, 12, 12]] \times 2$ 24 joint X logicals			BB $[[288, 12, 18]] \times 2$ 24 joint X logicals		
	Size	Deg	Time	Size	Deg	Time	Size	Deg	Time	Size	Deg	Time	Size	Deg	Time
Gauge	1.6k	9/13	0.46	1.6k	9/12	0.46	2.0k	9/13	0.53	3.1k	9/13	0.71	7.0k	9/14	1.60
Full-Opt	278/280	11/9	8.1	286/288	11/11	8.3	390/392	11/11	12.9	508/510	11/11	18.3	1.1k	13/12	53.5

**Figure 9.** Logical error rate simulation under circuit noise model. Green dot lines: physical error rate equal to logical error rate.**Table 4.** Scalability study on surface code

$[[441, 1, 21]]$			$[[1681, 1, 41]]$			$[[3721, 1, 61]]$			$[[6561, 1, 81]]$			$[[10201, 1, 101]]$		
Size	Deg	Time	Size	Deg	Time	Size	Deg	Time	Size	Deg	Time	Size	Deg	Time
149/150	12/12	7.26	360/361	12/12	23.04	777/778	12/12	42.36	1086/1087	12/12	69.51	1708/1709	12/12	103.81

logical error was observed within 10^6 samples. Across all tested configurations, including standalone BB codes and their combinations with surface and color codes, the optimized constructions by GeneCS (using Full-Opt) consistently achieve logical error rates that closely match those of the baseline (Gauge).

Notably, this performance is maintained despite a substantial reduction in ancillary resources (Tables 2 and 3). The logical error curves of the optimized codes nearly overlap

with those of the baseline across a wide range of physical error rates, indicating that error-correcting performance is preserved while significantly reducing qubit and check overhead. Overall, these results demonstrate that GeneCS improves resource efficiency without compromising reliability.

7.5 Scalability

We evaluate the scalability of our compiler on the surface code family with distances up to $d = 101$, as shown in Table 4. Our method scales to codes with more than 10^4 physical qubits while maintaining a constant maximum qubit and check degree of 12. The total runtime grows moderately with the code size, reaching approximately 10^2 seconds for the largest instance. Notably, this runtime corresponds to 100 independent samples during the construction process. Amortized over these samples, the average compilation time per instance is around one second, demonstrating the practical efficiency of our approach.

To further understand scalability, we analyze the theoretical complexity of our construction. The dominant cost arises from repeatedly estimating the second eigenvalue $\lambda_2(G)$ during graph construction. In the worst case, each estimation requires $O(n^3)$ time, and since we perform $O(n)$ such updates (due to constant-degree expansion), the overall worst-case complexity is $O(n^4)$. Despite this, our approach is significantly more efficient than prior methods that require exponential-time distance verification.

Remark 7.2. *Although our scalability evaluation focuses on surface codes, the results is expected to extend more broadly to other stabilizer codes. In particular, prior work has shown that irreducible logical operators in CSS stabilizer codes admit a locally repetitive structure analogous to that of the surface code [10]. Consequently, we expect the runtime and scaling behavior observed here to be broadly representative beyond the surface code setting.*

8 Related Work

Compared with the well-understood and highly optimized lattice surgery constructions for surface codes, code surgery for general stabilizer codes remains relatively new, and most existing works are primarily theoretical.

The first line of work focuses on general constructions with theoretical guarantees. Early work such as CKBB [8] preserves code distance but introduces low-distance gauge degrees of freedom, which require excessive thickening and lead to substantial overhead. Later gauge-fixing-based approaches [12] improve the construction pipeline, while [35] further provides theoretical guarantees on QLDPC structure, forming the basis for extensions such as extractors [22] and adapters [33]. In parallel, branching-based constructions have been proposed, initially based on CKBB [37] and later incorporating gauge-fixing techniques [11]. However, these approaches typically rely on conservative pipelines, resulting in large practical overhead.

The second line of work [9, 10, 25, 38] either does not provide guarantees on distance preservation or relies on computationally expensive procedures that do not scale to

large instances. Ensuring distance preservation in these approaches requires verification by solving computationally expensive problems (e.g., integer programming, or sparsest-cut problems), which do not scale to large codes. Moreover, such post-hoc verification does not ensure composability, as combining individually verified constructions during code communication may still violate distance preservation. Notably, recent work on parallel product surgery [21] approaches also require explicit distance checking to verify distance preservation, which can become computationally demanding for larger codes and higher target distances.

In contrast, our approach achieves both theoretical correctness and practical efficiency: it preserves code distance and QLDPC structure by construction, while significantly reducing overhead and scaling efficiently to large instances without requiring post-compilation verification, and ensuring that the resulting surgeries compose naturally.

Acknowledgements

We thank Zhiyang He (Sunny), Alexander Cowtan, Dominic J. Williamson, and Theodore J. Yoder for their insightful discussions and valuable feedback. This work was supported in part by the U.S. Department of Energy, Office of Science, Office of Advanced Scientific Computing Research under Contract No. DE-AC05-00OR22725 through the Accelerated Research in Quantum Computing Program MACH-Q project, the U.S. National Science Foundation CAREER Award No. CCF-2338773, and the Defense Advanced Research Projects Agency Microsystems Technology Office (MTO) HARQ Program under Agreement No. HR0011-26-9-E113. GL was also supported by a Cisco Research Award. This research was, in part, funded by the U.S. Government. The views and conclusions contained in this document are those of the authors and should not be interpreted as representing the official policies, either expressed or implied, of the U.S. Government.

References

- [1] Noga Alon, Asaf Nachmias, and Matan Shalev. 2022. The diameter of the uniform spanning tree of dense graphs. *Combinatorics, Probability and Computing* 31, 6 (2022), 1010–1030. doi:DOI:https://doi.org/10.1017/S0963548322000062
- [2] Arda Aydin, Nicolas Delfosse, and Edwin Tham. 2025. Cyclic Hypergraph Product Code. *arXiv preprint arXiv:2511.09683* (2025). doi:10.48550/arXiv.2511.09683
- [3] Héctor Bombín. 2013. An introduction to topological quantum codes. *arXiv preprint arXiv:1311.0277* (2013). doi:10.48550/arXiv.1311.0277
- [4] Sergey Bravyi, Andrew W Cross, Jay M Gambetta, Dmitri Maslov, Patrick Rall, and Theodore J Yoder. 2024. High-threshold and low-overhead fault-tolerant quantum memory. *Nature* 627, 8005 (2024), 778–782. doi:10.1038/s41586-024-07107-7
- [5] Nikolas P Breuckmann and Jens Niklas Eberhardt. 2021. Quantum low-density parity-check codes. *PRX quantum* 2, 4 (2021), 040101. doi:DOI:https://doi.org/10.1103/PRXQuantum.2.040101
- [6] Aranya Chakraborty and Daniel Gottesman. 2026. No-Go Theorem on Fault Tolerant Gadgets for Multiple Logical Qubits. doi:10.48550/arXiv.2602.13395 arXiv:2602.13395 [quant-ph]

- [7] Fan RK Chung. 1997. *Spectral graph theory*. Vol. 92. American Mathematical Soc. doi:10.1090/cbms/092
- [8] Lawrence Z Cohen, Isaac H Kim, Stephen D Bartlett, and Benjamin J Brown. 2022. Low-overhead fault-tolerant quantum computing using long-range connectivity. *Science Advances* 8, 20 (2022), eabn1717. doi:DOI:10.1126/sciadv.abn1717
- [9] Alexander Cowtan. 2024.SSIP: automated surgery with quantum LDPC codes. *arXiv preprint arXiv:2407.09423* (2024). doi:10.48550/arXiv.2407.09423
- [10] Alexander Cowtan and Simon Burton. 2024. CSS code surgery as a universal construction. *Quantum* 8 (2024), 1344. doi:10.22331/q-2024-05-14-1344
- [11] Alexander Cowtan, Zhiyang He, Dominic J Williamson, and Theodore J Yoder. 2025. Parallel logical measurements via quantum code surgery. *arXiv preprint arXiv:2503.05003* (2025). doi:DOI:https://doi.org/10.1103/gj8x-n5gg
- [12] Andrew W Cross, Zhiyang He, Patrick J Rall, and Theodore J Yoder. 2024. Improved QLDPC surgery: Logical measurements and bridging codes. *arXiv preprint arXiv:2407.18393* (2024). doi:10.48550/arXiv.2407.18393
- [13] Bryan Eastin and Emanuel Knill. 2009. Restrictions on Transversal Encoded Quantum Gate Sets. *Phys. Rev. Lett.* 102 (Mar 2009), 110502. Issue 11. doi:10.1103/PhysRevLett.102.110502
- [14] Xiang Fang, Jixuan Ruan, Sharanya Prabhu, Ang Li, Travis Humble, Dean Tullsen, and Yufei Ding. 2026. Bridging Superconducting and Neutral-Atom Platforms for Efficient Fault-Tolerant Quantum Architectures. doi:10.48550/arXiv.2601.10144 arXiv:2601.10144 [quant-ph]
- [15] Austin G Fowler and Craig Gidney. 2018. Low overhead quantum computation using lattice surgery. *arXiv preprint arXiv:1808.06709* (2018). doi:10.48550/arXiv.1808.06709
- [16] Austin G Fowler, Matteo Mariantoni, John M Martinis, and Andrew N Cleland. 2012. Surface codes: Towards practical large-scale quantum computation. *Physical Review A—Atomic, Molecular, and Optical Physics* 86, 3 (2012), 032324. doi:DOI:https://doi.org/10.1103/PhysRevA.86.032324
- [17] Michael Freedman and Matthew Hastings. 2021. Building manifolds from quantum codes. *Geometric and Functional Analysis* 31, 4 (2021), 855–894. doi:10.48550/arXiv.2012.02249
- [18] Joel Friedman. 2003. A proof of Alon’s second eigenvalue conjecture. In *Proceedings of the thirty-fifth annual ACM symposium on Theory of computing*. 720–724. doi:10.1145/780542.780646
- [19] Daniel Gottesman. 1997. *Stabilizer codes and quantum error correction*. California Institute of Technology. doi:10.48550/arXiv.quant-ph/9705052
- [20] Daniel Gottesman. 1998. Theory of fault-tolerant quantum computation. *Physical Review A* 57, 1 (1998), 127. doi:DOI:https://doi.org/10.1103/PhysRevA.57.127
- [21] Boren Gu, Andy Zeyi Liu, Armanda O Quintavalle, Qian Xu, Jens Eisert, and Joschka Roffe. 2026. QGPU: Parallel logic in quantum LDPC codes. *arXiv preprint arXiv:2603.05398* (2026).
- [22] Zhiyang He, Alexander Cowtan, Dominic J Williamson, and Theodore J Yoder. 2025. Extractors: QLDPC architectures for efficient Pauli-based computation. *arXiv preprint arXiv:2503.10390* (2025). doi:10.48550/arXiv.2503.10390
- [23] Shlomo Hoory, Nathan Linial, and Avi Wigderson. 2006. Expander graphs and their applications. *Bull. Amer. Math. Soc.* 43, 4 (2006), 439–561. doi:10.1090/s0273-0979-06-01126-8
- [24] Dominic Horsman, Austin G Fowler, Simon Devitt, and Rodney Van Meter. 2012. Surface code quantum computing by lattice surgery. *New Journal of Physics* 14, 12 (2012), 123011. doi:DOI10.1088/1367-2630/14/12/123011
- [25] Benjamin Ide, Manoj G Gowda, Priya J Nadkarni, and Guillaume Dauphinais. 2025. Fault-tolerant logical measurements via homological measurement. *Physical Review X* 15, 2 (2025), 021088. doi:DOI:https://doi.org/10.1103/PhysRevX.15.021088
- [26] Andrew J Landahl, Jonas T Anderson, and Patrick R Rice. 2011. Fault-tolerant quantum computing with color codes. *arXiv preprint arXiv:1108.5738* (2011). doi:10.48550/arXiv.1108.5738
- [27] Daniel Litinski. 2019. A game of surface codes: Large-scale quantum computing with lattice surgery. *Quantum* 3 (2019), 128. doi:10.22331/q-2019-03-05-128
- [28] Pranav S Mundada, Aleksei Khindanov, Yulun Wang, Claire L Edmunds, Paul Coote, Michael J Biercuk, Yuval Baum, and Michael Hush. 2026. Heterogeneous architectures enable a 138x reduction in physical qubit requirements for fault-tolerant quantum computing under detailed accounting. *arXiv preprint arXiv:2604.06319* (2026). doi:10.48550/arXiv.2604.06319
- [29] Michael A Nielsen and Isaac L Chuang. 2010. *Quantum computation and quantum information*. Cambridge university press. doi:10.1017/CBO9780511976667
- [30] Michael A. Perlin. 2023. qLDPC. <https://github.com/qLDPCOrg/qLDPC>.
- [31] Angelika Steger and Nicholas C Wormald. 1999. Generating random regular graphs quickly. *Combinatorics, Probability and Computing* 8, 4 (1999), 377–396. doi:DOI:https://doi.org/10.1017/S0963548399003867
- [32] Samuel Stein, Shifan Xu, Andrew W. Cross, Theodore J. Yoder, Ali Javadi-Abhari, Chenxu Liu, Kun Liu, Zeyuan Zhou, Charlie Guinn, Yufei Ding, Yongshan Ding, and Ang Li. 2025. HetEC: Architectures for Heterogeneous Quantum Error Correction Codes. In *Proceedings of the 30th ACM International Conference on Architectural Support for Programming Languages and Operating Systems, Volume 2* (Rotterdam, Netherlands) (ASPLOS ’25). Association for Computing Machinery, New York, NY, USA, 515–528. doi:10.1145/3676641.3716001
- [33] Esha Swaroop, Tomas Jochym-O’Connor, and Theodore J Yoder. 2024. Universal adapters between quantum LDPC codes. *arXiv preprint arXiv:2410.03628* (2024). doi:10.48550/arXiv.2410.03628
- [34] Fan Wang and Sandy Irani. 2025. Cycle Basis Algorithms for Reducing Maximum Edge Participation. *arXiv preprint arXiv:2511.10961* (2025). doi:10.48550/arXiv.2511.10961
- [35] Dominic J Williamson and Theodore J Yoder. 2024. Low-overhead fault-tolerant quantum computation by gauging logical operators. *arXiv preprint arXiv:2410.02213* (2024). doi:10.1038/s41567-026-03220-8
- [36] Theodore J Yoder, Eddie Schoute, Patrick Rall, Emily Pritchett, Jay M Gambetta, Andrew W Cross, Malcolm Carroll, and Michael E Beverland. 2025. Tour de gross: A modular quantum computer based on bivariate bicycle codes. *arXiv preprint arXiv:2506.03094* (2025). doi:10.48550/arXiv.2506.03094
- [37] Guo Zhang and Ying Li. 2025. Time-efficient logical operations on quantum low-density parity check codes. *Physical Review Letters* 134, 7 (2025), 070602. doi:10.1103/PhysRevLett.134.070602
- [38] Guo Zheng, Liang Jiang, and Qian Xu. 2025. High-Rate Surgery: towards constant-overhead logical operations. *arXiv preprint arXiv:2510.08523* (2025). doi:10.48550/arXiv.2510.08523
- [39] Junyu Zhou, Yuhao Liu, Ethan Decker, Justin Kalloor, Mathias Weiden, Kean Chen, Costin Iancu, and Gushu Li. 2026. TopoLS: Lattice Surgery Compilation via Topological Program Transformations. *arXiv preprint arXiv:2601.23109* (2026). doi:10.48550/arXiv.2601.23109

Algorithm 6: Ancilla Graph Construction

Step 1: Port Connecting. Let V_1 be a set of vertices with $|V_1| = |L|$, and construct a bijection f between L and V_1 .

Step 2: Expanding. Construct a base graph $G_1 = (V_1, E_1)$ as follows: (a). For each stabilizer $S \in \mathcal{S}$, recall that $K(S, L)$ is the set of qubits $q \in Q$ such that $S(q)$ and $L(q)$ anti-commute. Add a perfect matching $\mu(S, L)$ on $f(K(S, L))$, consisting of $|K(S, L)|/2$ edges, to G_1 . (b). Construct a constant-degree graph D on $|L|$ vertices with Cheeger constant $\beta_D \geq \beta$ for some constant β . Add the edges of D to G_1 .

Step 3: Decongestion. Apply the Decongestion Lemma (see Lemma A.0.2 in [17]) to obtain a cycle basis \mathcal{R} of G_1 with congestion ρ , together with a partition (see Corollary 15 in [22]) $\mathcal{R} = \bigcup_{i=1}^t P_i$ such that each P_i consists of edge-disjoint cycles and $t \leq O((\log |L|)^3)$.

Step 4: Thickening. Thicken G_1 by a factor $\ell = \max(t, 1/\beta)$ to obtain $G = G_1 \square J_\ell$, where $G = (V, E)$. This operation amplifies the relative Cheeger constant from β to $\ell\beta$, and spread the cycle basis to different level $G_1 \times \{r\}$.

Step 5: Cellulation. For each level $G_1 \times \{r\}$, triangulate every cycle in P_r to obtain a collection of triangles that generate the cycles in $P_r \times \{r\}$.

A Background on Graph-Based Code Surgery Construction

This section provides the formal background on graph-based code surgery constructions. These materials are included for completeness and are not required to understand the main contributions of the paper.

A.1 Graph Construction

We require the ancilla graph preserves the code distance, and that the deformed code remains a QLDPC code if the original code belongs to the QLDPC family. Prior work [22, 35] provides a theoretical procedure for constructing such graphs that satisfy these conditions, which we briefly introduce here. We first present several definitions.

Definition A.1 (Cheeger Constant and Relative Cheeger Constant [22]). *Let $G = (V, E)$ be an undirected graph. For any subset $U \subseteq V$, the edge boundary of U , denoted by $\delta(U)$, is defined as the set of edges with exactly one endpoint in U .*

The Cheeger constant $\beta(G)$ is defined as the largest real number such that, for all $U \subseteq V$,

$$|\delta(U)| \geq \beta(G) \cdot \min(|U|, |V \setminus U|).$$

Furthermore, for a subset $P \subseteq V$ and an integer $t > 0$, the relative Cheeger constant $\beta_t(G, P)$ is defined as the largest real

number such that, for all $U \subseteq V$,

$$|\delta(U)| \geq \beta_t(G, P) \cdot \min(t, |U \cap P|, |P \setminus U|).$$

In particular, the standard Cheeger constant is recovered as $\beta(G) = \beta_{|V|}(G, V)$. Both quantities are commonly referred to as measures of graph expansion, with larger values indicating better expansion.

Definition A.2 (Congestion [22]). *Let $G = (V, E)$ be a graph, and let R be a cycle basis of G . For each edge $e \in E$, let $\rho_R(e)$ denote the number of cycles in R that contain e . Define*

$$\rho = \max_{e \in E} \rho_R(e).$$

We say that R has congestion ρ , or that R is a ρ -basis.

Definition A.3 (Graph Thickening [22]). *Let $G_1 = (V_1, E_1)$ and $G_2 = (V_2, E_2)$ be two graphs. The Cartesian product of G_1 and G_2 is the graph*

$$G = G_1 \square G_2 = (V_1 \times V_2, E),$$

where

$$E = \{((u_1, u_2), (v_1, v_2)) : (u_1, v_1) \in E_1 \text{ or } (u_2, v_2) \in E_2\},$$

where in the first case we require $u_2 = v_2$, and in the second case $u_1 = v_1$. Let J_ℓ denote a path graph of length ℓ , consisting of ℓ vertices and $\ell - 1$ edges. We define the ℓ -fold thickening of G as the graph $G \square J_\ell$.

We refer to the ℓ copies of G in $G \square J_\ell$ as levels, and denote the r -th level by $G \times \{r\} = (V \times \{r\}, E \times \{r\})$ for $1 \leq r \leq \ell$.

The graph construction procedure is provided in Algorithm 6. For a logical operator L , we first construct a graph with only vertices and a port function f as shown in Step 1.

The purpose of Steps 2(b) and 4 is to ensure that logical operators in the original code Q , when dressed by the newly introduced stabilizers, do not suffer a reduction in weight, thereby preserving the code distance. Steps 3 and 4 ensure that each qubit participates in only a constant number of cycle checks, while Step 5 guarantees that each cycle check has constant weight.

An example is shown in Figure 10. Suppose the base graph has Cheeger constant 0.5 and admits three cycles in its cycle basis. By thickening the graph with $\ell = 2$, we obtain a graph with relative Cheeger constant $2 \cdot 0.5 = 1$, which meets the threshold required to preserve the code distance. Moreover, the cycle basis is distributed across levels such that cycles within each level are edge-disjoint, ensuring that each qubit participates in only a constant number of cycle checks (as illustrated in blue and yellow cycles in Figure 10(b)). Finally, the cellulation step reduces the cycle length (i.e., the weight of cycle checks) to 3 by decomposing cycles into triangles, as shown in Figure 10(c).

The graph constructed in this manner, together with the measurement protocol introduced in Definition 10 of [22], enables the measurement of logical operators of a code.

Bridge/Adapter. To enable logical operator measurements across codes, we introduce the notion of bridge/adapter. A

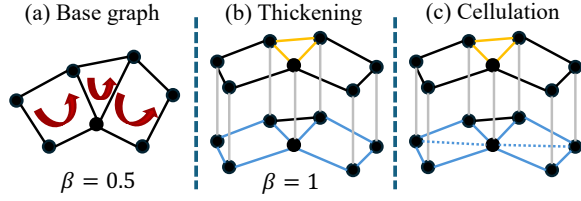


Figure 10. Graph Construction

bridge typically refers to a system that connects the measurement graphs of two codes within the same family, whereas an adapter connects measurement graphs between different code families.

Definition A.4 (Bridge/Adapter [33]). Let $G_1 = (V_1, E_1)$ and $G_2 = (V_2, E_2)$ be two graphs. A bridge/adapter between G_1 and

G_2 is defined as a set of pairwise non-overlapping edges B that connect vertices in V_1 to vertices in V_2 .

Suppose we aim to measure the joint logical operator L_1L_2 , where L_1 and L_2 correspond to codes \mathcal{Q}_1 and \mathcal{Q}_2 , respectively. The measurement procedure proceeds as follows. We first construct the measurement graphs G_1 and G_2 independently using Algorithm 6. We then set d to be the minimum code distance of the two codes, and connect exactly d vertices between the corresponding port sets P_1 and P_2 via an bridge/adapter. The additional cycle checks introduced by the bridge/adapter are included as stabilizers in the deformed code. As a result, the joint logical operator L_1L_2 is promoted to a stabilizer of the deformed code.